Prod. Eng. Res. Devel. (2012) 6:603–610
DOI 10.1007/s11740-012-0406-6

MACHINE TOOL

Thermal modelling of an HSC machining centre to predict thermal error of the feed system

Eckart Uhlmann · Jiangmin Hu

Received: 19 March 2012 / Accepted: 23 July 2012 / Published online: 4 August 2012

Abstract Machine tools equipped with linear motors can achieve high feed speed as well as high accuracy. However, the direct feed drive system generates heat through power loss and friction. In combination with environmental influences such as machine shop climate, this can lead to a local deformation of the machine tool structure and induce a direct positioning error. This paper presents a thermal model, using the finite element method, to simulate the thermal behaviour of a high-speed cutting machining centre equipped with linear motors. This model considers the complex boundary conditions such as heat sources, contact and convective heat transfer. Transient changes in temperatures and deformations are allowed in the solution. The comparison of the experiments show that this model can predict the temperature distribution and positioning error under specified operating conditions very well.

Keywords Machine tool · Thermal error · FEM

1 Introduction

The heat generated by continuous running of machine tools and the changes in environment cause thermal deformations of machine tools and in the end result in geometric inaccuracies of the workpiece. Thermal error can contribute up to 75 % of the total error [1, 2]. This is considered a major issue in production industries due to the high demand for micron precision in the workpiece. Machine tools equipped with linear motors can achieve high feed speed as well as accuracy. However, the linear motor operating at high speed can in turn generate a large amount of heat. The temperature of the primary part coil can increase up to $T = 120$ °C with power losses of $P = 2{,}600$ W [3]. Although most of the heat is dissipated by using the cooling system, the rest is transferred into the machine tool structure and environment. In addition, friction at contact areas of guideways also generates heat. The heat enters into the machine's discrete structure, passes through mechanical joints, and causes thermal deformations of the machine tool structure, which adversely affects the accuracy of machine tools [4]. Several studies have been published that focus on developing a thermal model in order to predict and optimise thermal behaviour of the linear motor itself using the finite element method (FEM) [3] or the finite difference method (FDM) [5]. Kim et al. [6] investigated thermal error in the linear-axes of a horizontal high-speed cutting centre with linear motors by means of experiments and an FEM model. However, the transient heat transfers between linear motors and machine structure, as well as the environmental influences that lead to thermal instability were not considered.

In this paper, a holistic 3D FEM thermal model of an high-speed cutting (HSC) machining centre equipped with linear motors is presented. This model considers heat generated by the power losses in linear motors and by friction of guideways, convection boundary conditions with ambient air, contact heat transfer between the component joints, and the thermal expansion of encoders. It can predict the transient temperature distribution of the machine structure and positioning error of the feed system. A series of experiments have been carried out to validate the thermal model. Good agreement of experimental data and calculated values demonstrates the

E. Uhlmann · J. Hu (✉)
Institute for Machine Tools and Factory Management (IWF),
Technische Universität Berlin, Pascalstraße 8-9,
10587 Berlin, Germany
e-mail: hu@iwf.tu-berlin.de

feasibility of the presented model for thermal error prediction.

2 Thermal model of the machine tool

2.1 The machine setup

The investigated machine tool, which has a symmetric gantry design, is the 5-axis HSC machining centre LPZ 500, developed by the company MAP GmbH, Magdeburg, Germany, as shown in Fig. 1. The machine tool equips linear motors for the linear axes and is able to realise feed speed of up to $v_f = 120$ m/min with an acceleration of $a = 25$ m/s^2. The linear scales are used to measure the actual position of linear axes.

2.2 FEM model

The FEM model of the machine tool was developed using the nonlinear finite element analysis software Marc made by the company MSC, Santa Ana, CA (USA), which is a combination of a heat transfer model and load-deformation model with thermal load [7], as shown in Fig. 2. This model has a total of 146,246 nodes and 133,173 elements, in which 3D 4-node tetrahedral and 8-node hexahedral heat transfer elements that are compatible with load-deformation analysis are used. Linear motors are simplified and represented as heat sources. The materials of all components are defined in the FEM model, as shown in Table 1.

The Marc software allows contact analysis to be performed automatically without the use of special contact elements. All of the components are defined as deformable

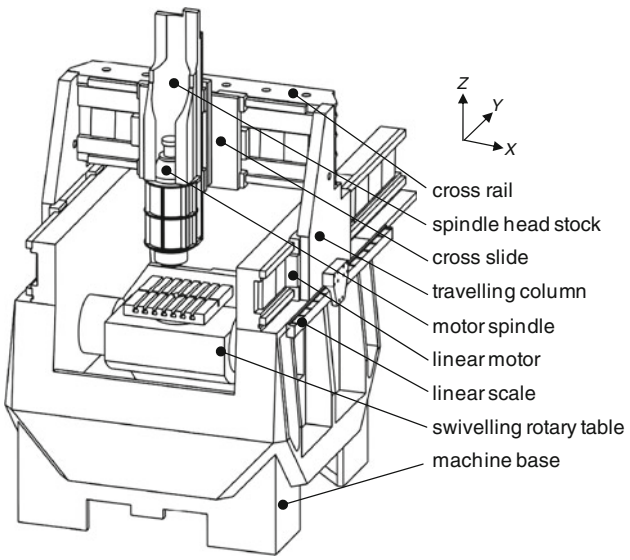

Fig. 1 HSC machining centre LPZ 500

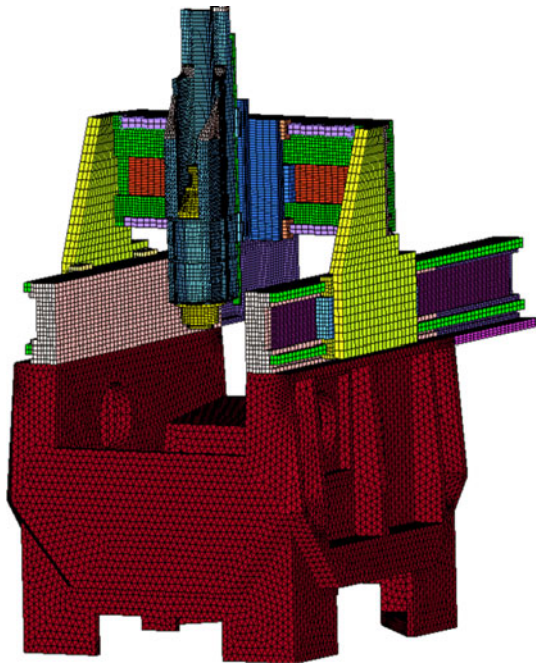

Fig. 2 FEM-model of the HSC machining centre LPZ 500

Table 1 Materials of the machine tool components

Components	Materials
Machine base	Cast iron
Travelling column	AlMgSi1
Cross rail	AlMgSi1
Cross slide	AlMgSi1
Spindle head stock	AlSi9Cu3
Linear guideway	58CrMoV4
Linear scale	Al, glass
etc.	Stainless steel

bodies using the "contact" option, which are simply a collection of finite elements. The nodes on the exterior surfaces are identified automatically as potential contact nodes. The program's rule of "optimize contact constraint equations" is used to determine the contact between the bodies [7]. While the "glue" option of contact is applied to connect independently meshed structure components, the "touching" option of contact is used to connect components that have relative motion in the direction tangential to the contacted components, i.e. the guideways.

The model of transient heat transfer is based on the heat conduction equation [8]:

$$\rho C_p \partial T/\partial t + k\nabla^2 T = \dot{P} \quad (1)$$

where T is the temperature distribution in space and time, ρ is the mass density, C_p is the specific heat capacity, ∇ is the gradient operator, k is the thermal conductivity, and $\dot{P}$ is the power density.

The load-deformation analysis computes deformations of the machine tool caused by thermal expansion. The general equation, based on Hookes's law, is as follows:

$$\varepsilon = \alpha \cdot \Delta T \tag{2}$$

where ε is the strain vector, α is the thermal expansion coefficient.

Some assumptions are made for the thermal modelling:

- Heat radiation to the surrounding is ignored.
- The temperature-dependent non-linear properties of the material (thermal conductivity, heat capacity, thermal expansion, etc.) are not considered, since the variation in room temperature condition is not significant.

2.3 Internal heat sources

Two major heat sources of the feed system are power losses in linear motors and friction of guideways. With the implementation of the cooling system based on the Thermo-Sandwich principle, the majority of heat generated by linear motors is dissipated through the coolant. Nevertheless, some heat is transferred to the machine tool structure [9]. Heat generation of the linear motors Q_v can be determined by mean of Siemens [9]:

$$Q_v = 3R_{str,20}[1 + 0.00393(T_N - 20)]I_{eff}^2 \tag{3}$$

where $R_{str,20}$ is the line resistance, T_N is the rated temperature and I_{eff} is the effective current. The heat $Q_{K,i}$ that is dissipated by the individual coolers is given by mean of Siemens [9]:

$$Q_{K,i} = Q_{K,MAX}\left(\frac{F_{eff}}{F_N}\right)^2 \tag{4}$$

where F_{eff} is the motor effective force, F_N is the rated force and $Q_{K,MAX}$ is the maximum dissipated heat output of each cooler. Therefore, the rest heat that is transferred to the machine tool structure Q_r can be calculated as:

$$Q_r = Q_v - \sum Q_{K,i} \tag{5}$$

Heat generation by friction of guideways Q_f can be defined by means of Eun [3]:

$$Q_f = (\mu F_m + f_d)v_f \tag{6}$$

where μ is the friction coefficient, which is between $\mu = 0.001$ and $\mu = 0.002$ in case of a ball-based guideway. F_m is the mean load of the guideway and f_d is the seal resistance.

Q_r and Q_f are modelled via heat fluxes and distributed to solid surfaces that are connected to heat sources.

2.4 Internal heat transfer

There are many joints in a machine tool. When two components are in contact, the presence of surface roughness produces imperfect contact at the joint, which results in a sharp temperature drop across the joint. Therefore, it is necessary to evaluate thermal contact conductance h_c at the contact surface of the components. It is assumed that the heat conduction through the actual contact spots and through the fluid in the gaps, are the two significant components of the heat transfer through a joint [10]. Therefore, the thermal contact conductance h_c can be defined as

$$h_c = h_s + h_g \tag{7}$$

where h_s is the contact spots conductance and h_g is the gap conductance. Cooper et al. [11] developed a theoretical thermal contact conductance model for contact surfaces. Various researchers in the thermal contact conductance field have used this model during the last few decades, and it has been shown that it is very accurate in general. Yovanovich [12] re-examined the model and proposed a new, more accurate correlation equation:

$$h_s = 1.25(k_s \tan\theta/\sigma)(p/H_c)^{0.95} \tag{8}$$

where k_s is the harmonic mean of the thermal conductivities of the joint, σ and tan θ are the effective root mean square roughness and the effective mean absolute slope of the combined profile of the two contacting surfaces, respectively. The apparent contact pressure is p, and H_c is the plastic contact hardness.

The simple correlation equation for the gap conductance model is given by Yovanovich [12, 13]:

$$h_g = \frac{k_g f_g}{B + \lambda\sigma} \tag{9}$$

where k_g is the thermal conductivity of the gas, f_g is the correlation factor, λ is the relative mean plane separation, and B is the complex gas gap rarefaction parameter.

Since the most commonly used connections in the machine tool are bolted joints, the contact pressure can be determined by means of Rieg et al. [14]:

$$p = \frac{nM_A}{\left(0.16S_p + \mu_{ges}\left(0.58d_2 + \frac{(d_h+d_w)}{4}\right)\right)A_k} \tag{10}$$

where n is the number of screws, M_A is the locking torque, S_p is the screw thread pitch, d_2 is the effective diameter of the thread, d_h is the bore diameter, d_w is the outer diameter of the washer face and A_k is the contact area. The variable μ_{ges} denotes the corresponding friction coefficient of the screw thread or the screw head.

2.5 External boundary condition

Machine tools exchange heat with the environment by convection. The heat transfer on the surface of the static structure component is through free convection, which is often caused by natural movement of air. Forced convection occurred on the surface of the moving component. Investigations of free convection have been carried out on vertical, horizontal and inclined plates and cylinders. Forced convection of parallel flow over a flat plate and flow across a cylinder and non-circular shapes have also been well studied [15, 16]. These results can be used as the convection boundary conditions in the FEM model of machine tools [17–19].

In the FEM model, a complete description of convection requires a definition of the heat transfer coefficient, ambient temperature, and surface temperature of the structure. The surface temperature of the structure is the result of the calculation via finite element analysis, while the ambient temperature is derived directly from measured values. The heat transfer coefficient depends upon physical properties of the fluid, the flow velocity and the surface geometry. The general equation determined by dimensional analysis in conjunction with experimental data is as follows:

$$h_f = Nu\frac{\lambda}{l} \tag{11}$$

where h_f is the convective heat transfer coefficient, Nu is the Nusselt number, λ is the thermal conductivity, and l is the characteristic length. For free convection, Nu is a function of the Rayleigh number Ra and Prandtl Pr number:

$$Nu = f(Ra, Pr) \tag{12}$$

For forced convection, the Nusselt number Nu is a function of the Reynold number Re and Prandtl number Pr:

$$Nu = f(Re, Pr) \tag{13}$$

In Tables 2 and 3 the summaries of correlations to calculate Nu for free and forced convection, respectively, are given. Hence, the corresponding coefficient for each surface of the machine tool structure can be calculated.

The heat transfer coefficients on the vertical surface of the cross rail for free and forced convection, respectively, have been chosen as calculated examples. The dependence of the coefficient for free convection on the ambient temperature can be seen in Fig. 3. The heat transfer coefficient for free convection is between 2.5 and 4.5 W/m^2/K. Figure 4 shows the dependence of the coefficient for forced convection on the feed speed, in which the value can be between 2.5 and 36 W/m^2/K. The coefficient rises sharply with increasing feed speed.

In this paper, an extended program is used to determine heat transfer coefficients and Fig. 5 shows the simulation procedure for adapting them. On the basis of the structure's surface temperature, temperature-dependent air physical properties, feed speed, and the ambient temperature, the heat transfer coefficients are calculated anew after each time step and adapted to the next step in time to define the new boundary conditions during the thermal simulation. Temperature-dependent air physical properties and feed speed are read from tables via linear interpolation.

3 Transient simulation

Heat transfer analysis is used for computing the temperature development, while stress analysis predicts deformations caused by thermal expansion. In this section, the feed movement of the Y-axis is simulated as the selected example. It is assumed that, the Y-axis traverses between $Y = -200$ mm and $Y = 400$ mm at a feed speed of $v_f = 70$ m/min during a given time of $t = 240$ min. The initial temperature of the machine structure is $T = 24$ °C and the ambient temperature of $T = 24.6$ °C is a constant value during the simulation. The constant step time of $t_n = 5$ min with steps of $n = 48$ are set for the transient simulation. The maximum nodal temperature change of $\Delta T = 50$ °C is allowed before matrices are reassembled per increment.

Figure 6 shows the simulated temperature distribution of the machine at the end of the feed movement of the Y-axis. The temperature of the machine tool increases during the feed movement, but this increase is not significant. The highest temperature of only $\Delta T = 1.2$ °C arises in the columns, which are near the heat sources of the linear motors. This is mainly because of the powerful cooling systems of the linear motors, which dissipate most of the heat.

Figure 7 shows the machine deformation due to the temperature distribution. The maximum displacement appeared at the cross slide. The TCP-displacements of $\Delta X = 0.1$ µm, $\Delta Y = 12$ µm and $\Delta Z = 5$ µm arise while taking the linear motor's cooling system into account. Due to the symmetric construction of the machine, there are nearly no displacement in the X-direction of the TCP.

Two types of offset are combined with the thermal induced positioning error of the feed system. The first is the thermal induced TCP-displacement Δi_{TCP}. The second offset is the thermal deformation of encoders, which is because of the thermal expansion of the linear scale Δi_{scale} and the thermal displacement of the point of the machine tool slide Δi_{reader} at which the encoder reader is fixed [6]. The total thermal positioning error Δi_{total} can be defined as

Table 2 Summary of free convection correlations for flow on plates and cylinders [15–17]

Convection form	Conditions	Correlation	
The top surface of the hot horizontal plate and the bottom surface of the cold horizontal plate	$10^4 \le Ra \le 10^7$	$Nu = 0.54Ra^{0.25}$	(14)
	$10^7 \le Ra \le 10^{11}$	$Nu = 0.15Ra^{0.33}$	(15)
The top surface of the cold horizontal plate and the bottom surface of the hot horizontal plate	$10^5 \le Ra \le 10^{10}$	$Nu = 0.27Ra^{0.25}$	(16)
The vertical Plate	$10^{-1} \le Ra \le 10^{12}$	$Nu = \left\{0.825 + \frac{0.387Ra^{1/6}}{\left[1+(0.492/\mathrm{Pr})^{9/16}\right]^{8/27}}\right\}^2$	(17)
The top surface of the cold inclined plate and the bottom surface of the hot inclined plate	$10^{-1} \le Ra \le 10^{12}$	$Nu = \left\{0.825 + \frac{0.387(Ra\cos\gamma)^{1/6}}{\left[1+(0.492/Pr)^{9/16}\right]^{8/27}}\right\}^2$	(18)
The top surface of the hot inclined plate and the bottom surface of the cold inclined plate	$10^{-1} \le Ra \le 10^{12}$	$Nu = 0.56(Ra_c\cos\gamma)^{0.25} + 0.13\left(Ra^{0.33} - Ra_c^{0.33}\right)$ $Ra_c = 10^{(8.9-0.00178\gamma^{1.82})}$	(19)
The vertical cylinder	$10^{-1} \le Ra \le 10^{12}$	$Nu = \left\{0.825 + \frac{0.387Ra^{1/6}}{\left[1+(0.492/\mathrm{Pr})^{9/16}\right]^{8/27}}\right\}^2 + 0.97\frac{H}{D}$	(20)
The horizontal cylinder	$10^{-1} \le Ra \le 10^{12}$	$Nu = \left\{0.6 + \frac{0.387Ra^{1/6}}{\left[1+(0.559/Pr)^{9/16}\right]^{8/27}}\right\}^2$	(21)

Table 3 Summary of forced convection correlations for flow on plates and cylinders [15–17]

Convection form	Conditions	Correlation	
The flat plate in parallel flow	$Re < 10^5$ $0.6 < Pr < 2{,}000$	$Nu_{lam} = 0.664Re^{0.5}Pr^{1/3}$	(22)
	$5{\cdot}10^5 < Re < 10^7$ $0.6 < Pr < 2{,}000$	$Nu_{turb} = \frac{0.037Re^{0.8}Pr}{1+2.443Re^{-0.1}(Pr^{2/3}-1)}$	(23)
The flat plate in overflowed flow	$10 < Re < 10^7$	$Nu = \sqrt{Nu_{lam}^2 + Nu_{turb}^2}$	(24)
The flat plate in cross flow	$4{\cdot}10^3 < Re < 1.5{\cdot}10^4$ $0.6 < Pr < 1{,}000$	$Nu = 0.228Re^{0.731}Pr^{1/3}$	(25)
The cylinder in cross flow	$10^1 < Re < 10^7$ $0.6 < Pr < 1{,}000$	$Nu = 0.3 + \sqrt{Nu_{lam}^2 + Nu_{turb}^2}$ Nu_{lam} = Eq. (22) and Nu_{turb} = Eq. (23)	(26)

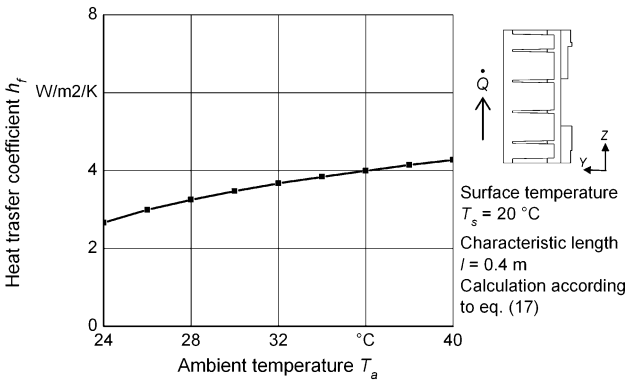

Fig. 3 Effect of the ambient temperature on free convection on the vertical surface of the cross rail

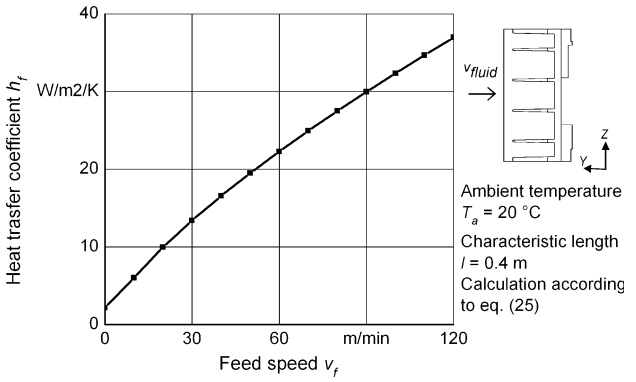

Fig. 4 Effect of the feed speed on forced convection on the vertical surface of the cross rail

$$\Delta i_{total} = \Delta i_{TCP} + \Delta i_{reader} + \Delta i_{scale} \quad (27)$$

where i is the moving axis. Figure 8 shows the simulated thermal error development of position $Y = 400$ mm by moving the Y-axis. Due to the increase of the displacements $\Delta Y_{TCP} = 13$ µm and $\Delta Y_{reader} = 5$ µm, the total thermal positioning error is $\Delta Y_{total} = 18$ µm at the end of a feed movement of $t = 240$ min.

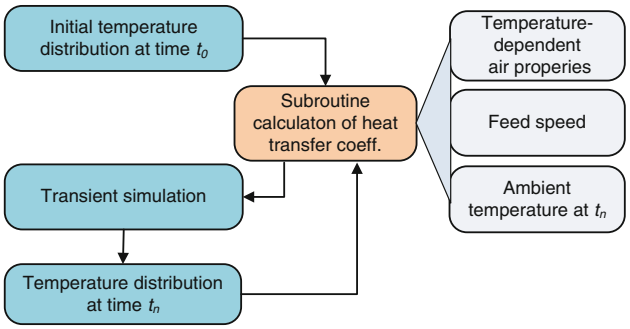

Fig. 5 Simulation procedure with the subroutine to calculate the heat transfer coefficients

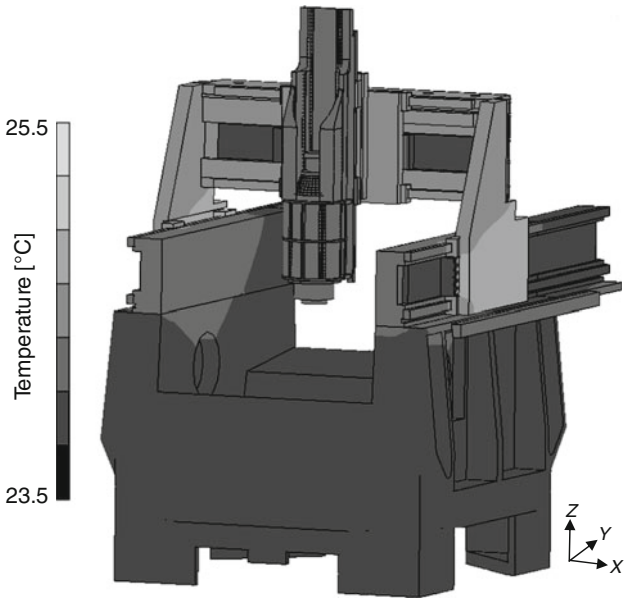

Fig. 6 Simulated temperature distribution of the machine tool structure at the end of the feed movement ($t = 240$ min)

4 Experimental verification

In order to verify this thermal model, a series of tests were done at different environmental conditions to measure the thermal drift of the Y-axis with the laser interferometer. According to ISO 230-3, the Y-axis traversed between $Y = -210$ mm and $Y = 410$ mm for $t = 240$ min with a feed speed of $v_f = 70$ m/min. The target positions are $Y = -200$ mm and $Y = 400$ mm. The dwell time at each target position is set to $t = 1$ s. Bi-directional measurements were used to minimise the reversal error. The temperatures of the machine tool and ambient air were measured during the axis cycling every 1 min with thermocouples type K. Five sensors were placed on the linear scale, the column close to primary part of linear motor, the machine bed, and the spindle head, as shown in Fig. 9. A sensor in the work space near the spindle head was used to measure the ambient temperature.

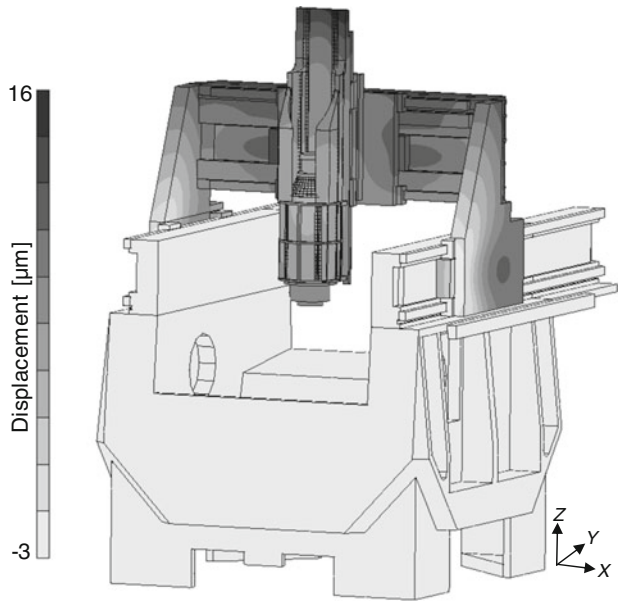

Fig. 7 Simulated thermal deformation of the machine tool structure at the end of the feed movement ($t = 240$ min)

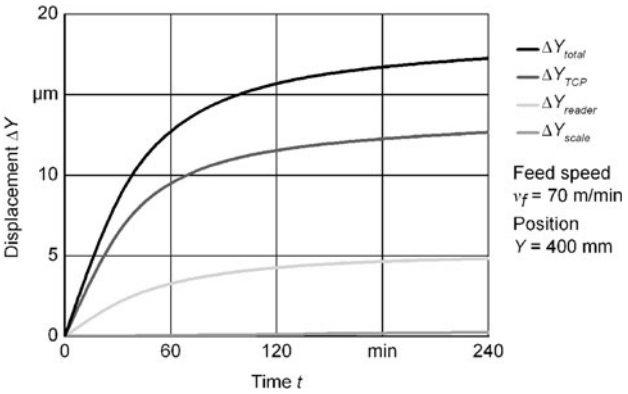

Fig. 8 Example of simulated thermal error development of position $Y = 400$ mm by moving Y-axis

The measured and simulated temperature variations at different environmental conditions are shown in Figs. 10 and 11. Here, Fig. 10 represents a variable ambient temperature from $T = 25.5$ to $T = 26.8$ °C, while Fig. 11 considers a constant ambient temperature of $T = 24.6$ °C. It can be seen clearly that calculated temperature variations from FEM are very close to the measured data of both tests. The deviation is less than 2 %. In comparison with Fig. 11, Fig. 10 shows how a rapid environmental variation can cause temperature changes of the machine tool structure. With the rise of ambient temperature, the temperatures of machine tool components increase sharply, which cannot be seen at constant environmental condition.

Figures 12 and 13 show the comparison between the measured and simulated positioning error of the Y-axis in the condition of variable and constant ambient temperature,

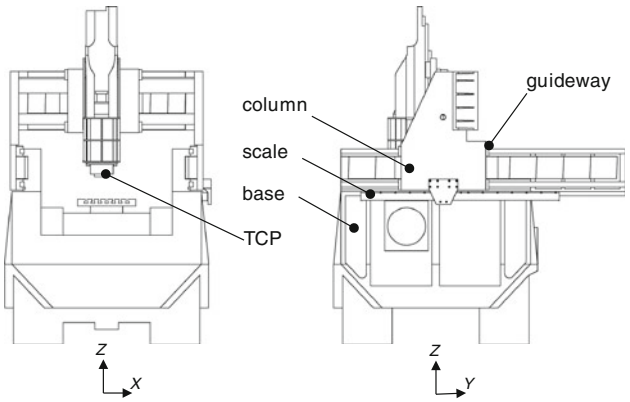

Fig. 9 Layout of the experimental thermocouples

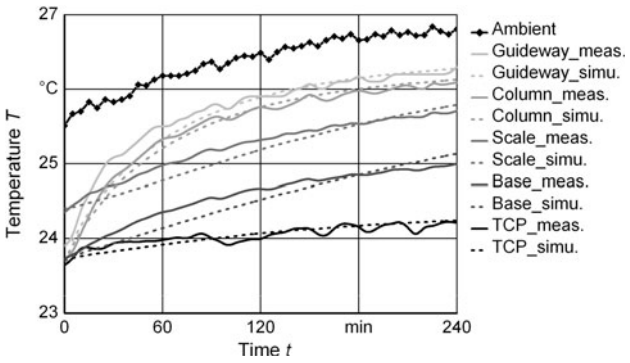

Fig. 10 Comparison of measured and simulated temperature variations of the machine structure by moving Y-axis at $v_f = 70$ m/min in the condition of variable ambient temperature

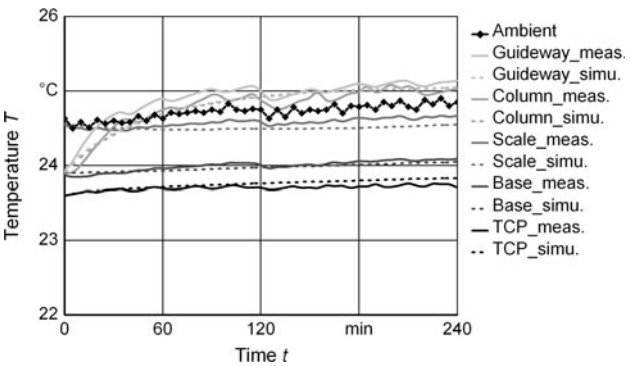

Fig. 11 Comparison of measured and simulated temperature variations of the machine structure by moving Y-axis at $v_f = 70$ m/min in the condition of constant ambient temperature

respectively. The simulated positioning errors match the measured values very well. In case of the variable ambient temperature condition, with increasing ambient temperature the positioning error increases continually up to $\Delta Y_1 = -36$ μm at the end of measuring time. In contrast, in case of the constant ambient temperature condition, the positioning error increases rapidly to the maximum value

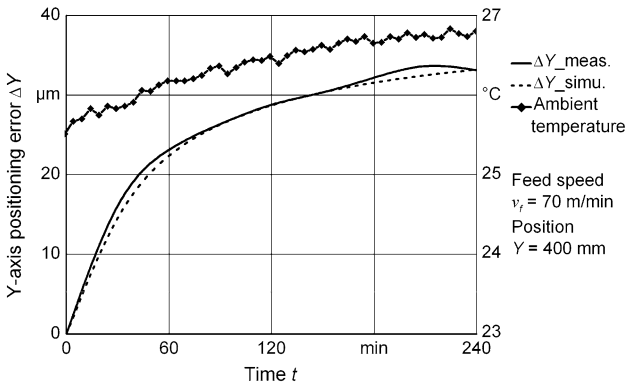

Fig. 12 Comparison of the measured and simulated positioning error of the Y-axis in the condition of variable ambient temperature

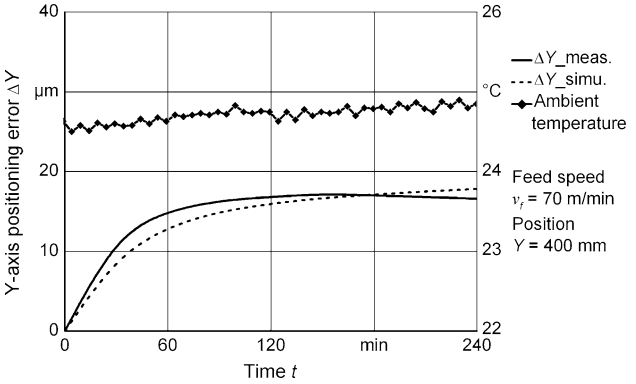

Fig. 13 Comparison of the measured and simulated positioning error of Y-axis in the condition of constant ambient temperature

of $\Delta Y_2 = -18$ μm after approximately 60 min. Subsequently, the displacement remains constant until the end of measuring time. These results confirm that the ambient temperature variation plays an important role in thermal error progression during movement of linear axes.

5 Summary and conclusions

This paper deals with the thermal induced positioning error prediction of a machine tool. First, the FEM model of the HSC machining centre equipped with linear motors is presented. Power losses in linear motors and friction of guideways are considered as the internal heat sources. Convection boundary conditions with ambient air and thermal contact conductance between joints are evaluated as accurately as possible. Afterwards, transient thermal distribution and positioning error of the feed system in a machine tool it induces are analysed. Finally, the validation of the presented model is performed by using temperature and displacement measurements. The comparison between measured and simulated results shows very good agreement.

In the future, simulation-based sensitivity analyses focusing on the description of boundary conditions will be conducted in order to improve the simulation results.

References

1. Weck M, McKeown P, Bonse R et al (1995) Reduction and compensation of thermal errors in machine tools. CIRP Ann 44(2):589–598
2. Bryan J (1990) International status of thermal error research. CIRP Ann 39(2):645–656
3. Eun I (1999) Optimierung des thermischen Verhaltens von elektrischen Linearmotoren für den Einsatz in Werkzeugmaschinen. In: Berichte aus der Produktionstechnik, vol 29. Shaker, Aachen
4. Uhlmann E, Hu J (2010) Simulation of the thermal behavior of a machine tool equipped with linear motors. Deutsch-Polnisches Seminar 2010
5. Raffi S (2000) Optimierung des thermischen Verhaltens von direktangetriebenen Vorschubsystemen. In: Darmstädter Forschungsberichte für Konstruktion und Fertigung. Shaker, Aachen
6. Kim J, Jeong YH, Cho D (2004) Thermal behavior of a machine tool equipped with linear motors. Int J Mach Tools Manuf 44(7–8):749–758
7. MSC software Manuals (2008) Marc volume A: theory and user information
8. Baehr D, Stephan K (2009) Wärme- und Stoffübertragung. Springer, Berlin
9. Siemens Manuals (2009) SINAMICS drive technologies peak and continuous load motors in the 1FN3 product family
10. Madhusudana C (1996) Thermal contact conductance. Springer, New York
11. Cooper G, Mikic B, Yovanovich M (1969) Thermal contact conductance. Int J Heat Mass Transf 12(3):279–300
12. Yovanovich M (1981) New contact and gap conductance correlations for conforming rough surfaces. In: AIAA Paper No. 81-1164, AIAA 16th Thermophysics Conference, Palo Alto, CA, June 23–25, pp 1–6
13. Negus J, Yovanovich M (1988) Correlation of gap conductance integral for conforming rough surfaces. J Thermophys Heat Transf 2(3):279–281
14. Rieg F, Kaczmarek M (2006) Taschenbuch der Maschinenelemente. Carl Hanser, München
15. Gesellschaft VDI (ed) (2006) VDI-Wärmeatlas, 10th edn. VDI-Buch. Springer, Berlin
16. Incropera FP, DeWitt DP, Bergman TL, Lavine AS (2007) Fundamentals of heat and mass transfer, 6th edn. Wiley, New York
17. Hoffmann E (1988) Konvektiver Wärmeübergang an arbeitsseitigen Spindelstockwänden. Produktionstechnik—Berlin, Forschungsberichte für die Praxis, vol 66. Carl Hanser, München
18. Zäh M, Maier T (2010) Simulation des thermischen Maschinenverhaltens. Zeitschrift für wirtschaftlichen Fabrikbetrieb 105(7–8):655–659
19. Gleich S. (2008) Simulation des thermischen Verhaltens spanender Werkzeugmashcinen in der Entwurfsphase. PhD thesis, Technischen Universität Chemnitz